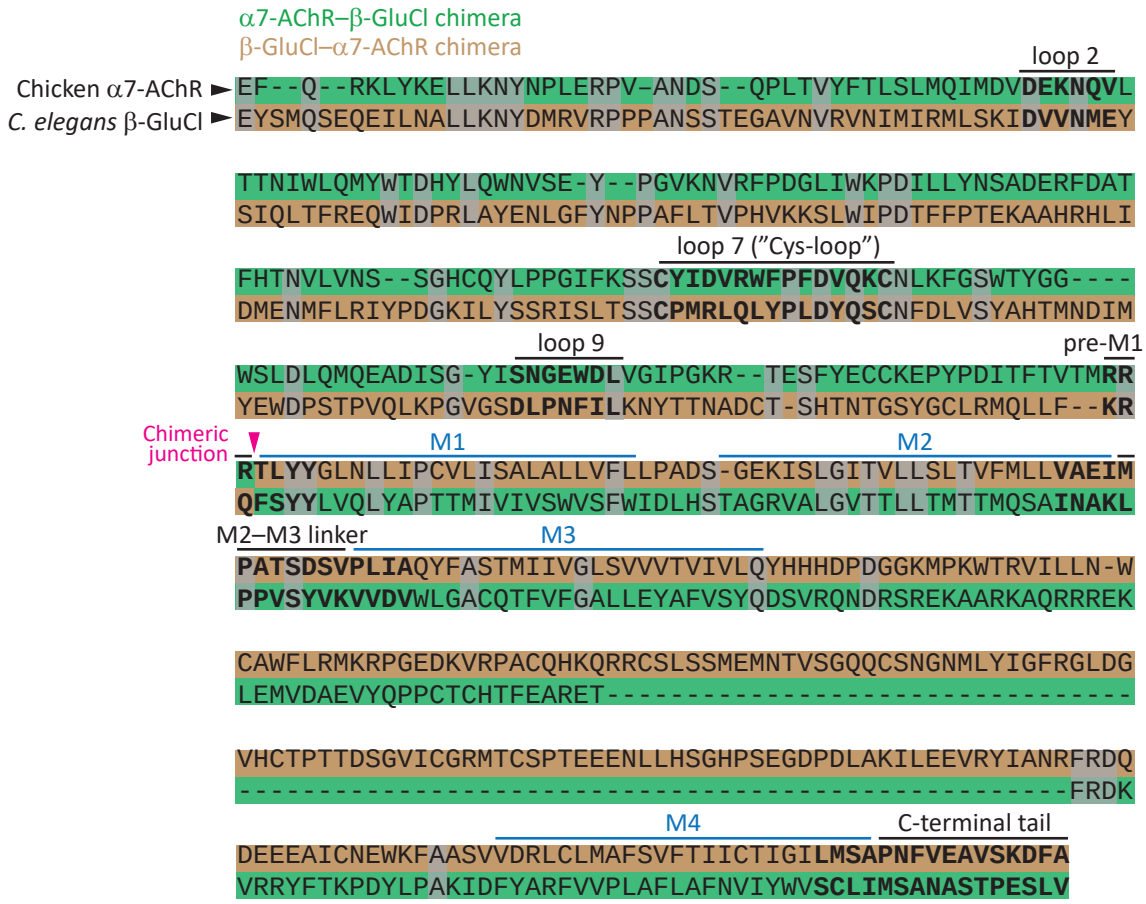

Fig. S1. Alignment of α7-AChR and β-GluCl sequences. The top sequence corresponds to the α7-AChR from chicken, and the bottom one corresponds to β-GluCl from *C. elegans*. The sequence of the α7-AChR–β-GluCl ECD–TMD chimera is indicated with a green background, and that of the reverse construct is indicated with a dark-yellow background; identical residues are indicated with a superimposed gray background. Residues that, on the basis of atomic models of other pLGICs, are expected to be at the ECD–TMD interface are indicated in bold. The alignment was generated in ClustalW using 15 sequences that (in addition to those of the chicken α7-AChR and *C. elegans* β-GluCl) also included *C. elegans* α1-GluCl; mouse α1-, β1-, δ-, and ε-AChR; mouse 5-HT_{3A}R; rat α1-, β1-, and γ2-γ-aminobutyric-acid type-A receptor; rat α1- and β-GlyR; and the bacterial GLIC and ELIC. Disregarding the highly variable M3–M4 linker, the sequences of chicken α7-AChR and *C. elegans* β-GluCl are 17.7 % identical (28.6 % similar). For comparison, the mouse-muscle AChR (the average of the four adult-type subunits) and the bacterial pLGIC GLIC are 19 % identical (33 % similar); the mouse-muscle AChR and the—also bacterial—ELIC are 16.9 % identical (30.4 % similar); and GLIC and ELIC are 20.5 % identical (35.8 % similar). For all pairwise sequence comparisons, the identity and similarity are higher when calculated only for the structural elements at the ECD–TMD interface.

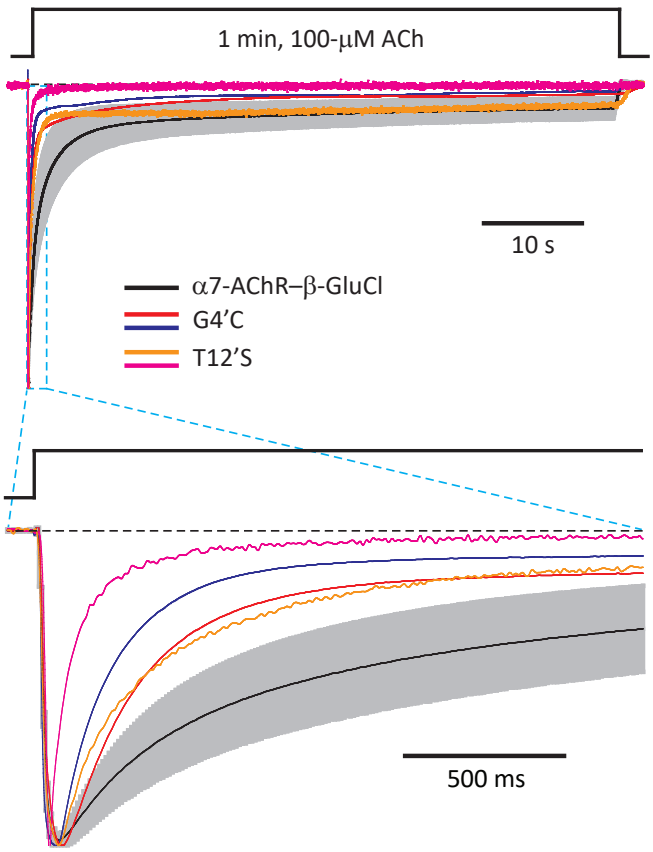

Fig. S2. Mutations in M2 speed up desensitization of the α7-AChR–β-GluCl CS chimera. Much as they do in the background of the PPSV→AAAA mutant, the M2 mutations G4'C and T12'S accelerated the time course of entry into desensitization of the CS construct. Normalized inward currents recorded in the whole-cell configuration under asymmetrical KCl-concentration conditions in response to the application of 1-min pulses of 100-μM ACh. The membrane potential was ~–60 mV. Black dashed lines denote the zero-current baseline. Two representative responses from each mutant are shown. Each displayed response was recorded from a different cell. For comparison, the averaged response (mean ± 1SD) of the CS chimera (without any additional mutation) to 1-min pulses of 100-μM ACh is also shown, as in Fig. 2*D* (mean: black solid line; SD: gray error bars).

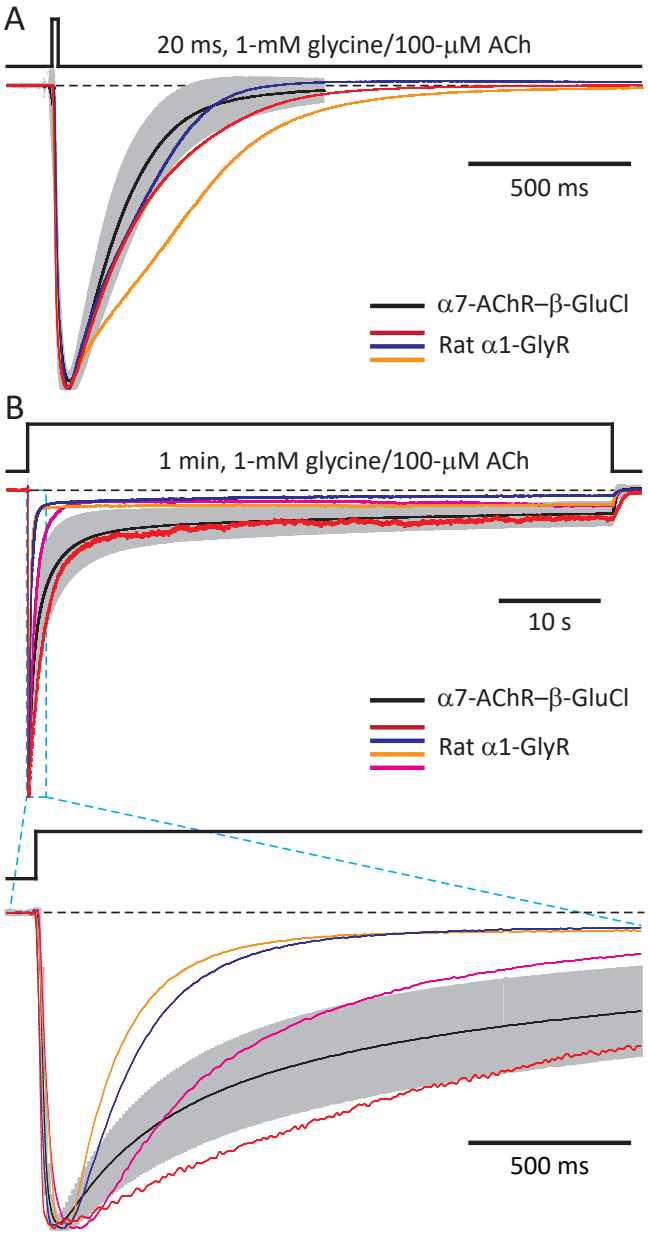

Fig. S3. The gating kinetics of the α7-AChR–β-GluCl CS chimera are similar to those of the rat α1-GlyR. Normalized inward currents recorded from the rat α1-GlyR in the whole-cell configuration under asymmetrical KCl-concentration conditions in response to the application of 20-ms or 1-min pulses of 1-mM glycine. The membrane potential was ~–60 mV. Black dashed lines denote the zero-current baseline. (*A*, *B*) Three representative responses to 20-ms pulses, and four to 1-min pulses, are shown. Each displayed response was recorded from a different cell. For comparison, the averaged responses (mean ± 1SD) of the CS chimera (without any additional mutation) to 20-ms or 1-min pulses of 100-μM ACh are also shown , as in Fig. 2 *C* and *D* (mean: black solid line; SD: gray error bars).

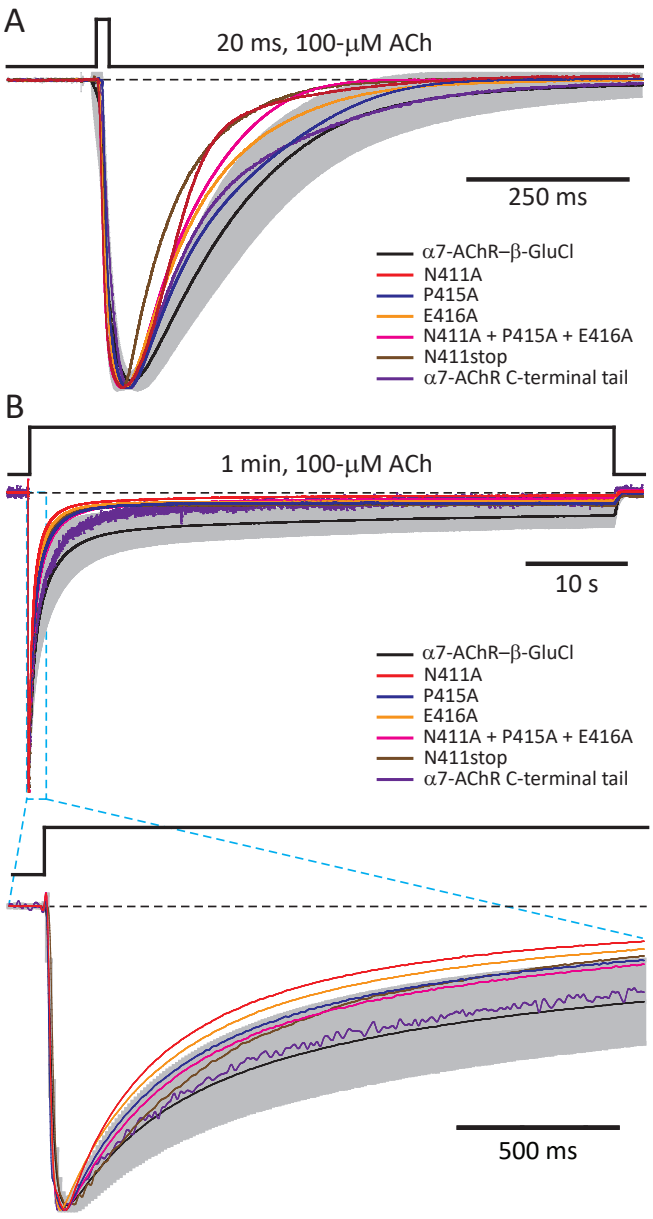

Fig. S4. Probing the effect of mutations to the C-terminal tail on gating. Normalized inward currents recorded from the indicated CS-chimera mutants in the whole-cell configuration under asymmetrical KCl-concentration conditions in response to the application of 20-ms or 1-min pulses of 100-μM ACh. The membrane potential was ~–60 mV. Black dashed lines denote the zero-current baseline. (*A*, *B*) One representative response from each mutant is shown. For comparison, the averaged responses (mean ± 1SD) of the CS chimera (without any additional mutation) to 20-ms or 1-min pulses of 100-μM ACh are also shown , as in Fig. 2 *C* and *D* (mean: black solid line; SD: gray error bars).

Table S1. Characterization of α7-AChR–β-GluCl CS-chimera mutations

Structural element/ wild-type sequence	Mutation(s)	Mutated sequence*	Function†	Cell-surface expression mutant-to-CS ratio (mean ± SE) (replicates)
Loop 2 D66EKNQV	D66A + E67A + N69A + Q70A	A66AKAAV	Yes	0.011 ± 0.0068 (4)
	β-GluCl loop 2	D66VVNME	Yes	1.3 ± 0.078 (4)
Loop 7 C150YIDVRWFPFDVQKC	W156A	C150YIDVRAFPFDVQKC	Yes	0.69 ± 0.057 (4)
	F157A	C150YIDVRWAPFDVQKC	No	0.35 ± 0.11 (12)
	P158A	C150YIDVRWFAFDVQKC	No	Undetectable (4)
	P158Q	C150YIDVRWFQFDVQKC	No	0.0052 ± 0.00075 (4)
	P158G	C150YIDVRWFGFDVQKC	No	0.010 ± 0.0038 (4)
	D160A	C150YIDVRWFPFAVQKC	Yes	0.047 ± 0.012 (4)
	Q162A	C150YIDVRWFPFDVAKC	Yes	0.71 ± 0.062 (4)
	D160A + Q162A	C150YIDVRWFPFAVAKC	No	0.0096 ± 0.0041 (4)
	β-GluCl Cys-loop	C150PMRLQLYPLDYQSC	Yes	0.15 ± 0.010 (4)
Loop 9 S192NGEWDL	N193A	S192AGEWDL	Yes	0.54 ± 0.019 (4)
	G194A	S192NAEWDL	Yes	1.2 ± 0.15 (4)
	E195A	S192NGAWDL	Yes	0.33 ± 0.0088 (4)
	W196A	S192NGEADL	No	0.0025 ± 0.0017 (4)
	G194P + E195N + W196F	S192NPNFDL	No	0.084 ± 0.0026 (4)
	L198A	S192NGEWDA	Yes	0.053 ± 0.0046 (4)
Pre-M1 linker R227RR	R227A + R229A	A227RA	Yes	0.018 ± 0.0029 (4)
	β-GluCl pre-M1	K227RQ	Yes	0.17 ± 0.010 (4)
	R228A	R227AR	No	0.0023 ± 0.00019 (4)
	Arg insertion	R227RRR	No	0.66 ± 0.0084 (4)
N-terminus of M1 F230SYY	Y232A + Y233A	F230SAA	Yes	0.78 ± 0.055 (4)
M2–M3 linker L284PPVSYVK	P285A + P286A + S288A + V290A	L284AAVAYAK	Yes	0.53 ± 0.056 (4)
	α7-AChR M2–M3 linker	M284PATSDSV	No	1.5 ± 0.10 (4)
	α7-AChR M2–M3 linker + D289K	M284PATSKSV	No	2.0 ± 0.083 (4)
	P285A + P286A + S288A + V290A + G266C	L284AAVAYAK and M2 G4'C	Yes	0.99 ± 0.075 (4)
	P285A + P286A + S288A + V290A + T274S	L284AAVAYAK and M2 T12'S	Yes	0.14 ± 0.014 (4)
C-terminal tail M408SANASTPESLV	N411A	M408SAAASTPESLV	Yes	1.2 ± 0.056 (3)
	P415A	M408SANASTAESLV	Yes	1.4 ± 0.13 (3)
	E416A	M408SANASTPASLV	Yes	1.0 ± 0.10 (3)
	N411A + P415A + E416A	M408SAAASTAASLV	Yes	1.1 ± 0.076 (3)
	N411stop	M408SA	Yes	0.74 ± 0.036 (3)
	α7-AChR C-terminal tail	P408NFVEAVSKDFA	Yes	0.27 ± 0.033 (3)

*Mutated residues are underlined.

†For some mutants, poor expression on the plasma membrane may underlie the failure to observe currents in response to ACh applications.